Analysis of the 1 Year Outdoor Performance of Quantum Dot Luminescent Solar Concentrators

Thomas A de Bruin, Raimon Terricabres-Polo, Annanta Kaul, Natalia K. Zawacka, P. Tim Prins, Thomas F. J. Gietema, Anne C. de Waal, Dick K. G. de Boer, Daniel A. M. Vanmaekelbergh, Paul Leblans, Stijn Verkuilen, Zeger Hens, Celso de Mello Donega, and Wilfried G. J. H. M. van Sark*

Three quantum dot luminescent solar concentrators (QDLSCs) are constructed to assess their performance in an outdoor environment over an entire year. The QDLSCs have a $45 \times 50 \times 1.2 \, cm^3$ PMMA-Kraton-PMMA sandwich structure with either InP/ZnSe/ZnS, $CuInS_2$/ZnS, or CdSe/CdS/ZnS core/shell quantum dots incorporated in the Kraton interlayer. Furthermore, two reference LSCs are included: one using Lumogen F Red 305 as the luminophore and one without a luminophore in the Kraton layer. The power conversion efficiency is assessed for a cloudy and a sunny day, showing the influence of diffuse and direct irradiance. Moreover, the influence of mounting orientation and direct irradiance is analyzed for individual solar strips attached to the sides. Long-term results show an efficiency increase of $CuInS_2$/ZnS and InP/ZnSe/ZnS QDLSC while the CdSe/CdS/ZnS QDLSCs and the Lumogen LSC show a pronounced drop in efficiency in the first 3 months. Photodegradation studies under continuous white light exposure for 420 h are performed on smaller pieces cut from the QDLSCs before their assembly outdoors and show similar trends to those observed in the 1 year outdoor study. Future research will focus on the postmortem analysis of the QDLSCs and increasing the efficiencies.

1. Introduction

The luminescent solar concentrator (LSC) as a power-generating window is a solution for the lack of appropriate horizontal space in densely populated areas.[1,2] The advantages of the LSC are its performance under diffuse irradiance[3] and the flexibility in color.[4] Recently, LSCs have been increasingly using semiconductor nanocrystals.[5] These nanocrystals, often called quantum dots (QD), function as a luminophore inside the LSC.[6] The QDs are attractive because of their broad absorption bands, high quantum yields (QYs), and easy-to-tune bandgap.[7] **Figure 1** shows the working principles of an LSC and the loss mechanisms present.

Over the past decade, the popularity of QD-based LSCs (QDLSCs) has equaled that of LSCs based on organic dyes.[8] However, most of the presented results are for small-area LSCs[5], which are too small for actual window applications. Furthermore, there are a limited number of studies on the performance and stability under working conditions. Indoors, Bomm et al. showed that CdSe QDLSCs could perform steadily for 300 h under constant illumination.[9] Liu et al. also reported on the steady performance of a CdSe QDLSC under constant illumination for 7 h,[10] taking into account temperature fluctuations. For Cd-free devices, Anand et al. fabricated a $CuInS_2$ QDLSC with a constant optical efficiency after 120 h of UV light exposure.[11] Makarov et al. reported the outdoor power output of $CuInS_2$ QDLSCs as a function of daytime and the cardinal orientation

T. A. de Bruin, A. Kaul, T. F. J. Gietema, A. C. de Waal, W. G. J. H. M. van Sark
Copernicus Institute of Sustainable Development
Utrecht University
Princetonlaan 8a, 3584, CB, Utrecht, The Netherlands
E-mail: w.g.j.h.m.vansark@uu.nl

R. Terricabres-Polo, P. T. Prins, D. K. G. de Boer,
D. A. M. Vanmaekelbergh, C. de Mello Donega
Debye Institute for Nanomaterials Science
Utrecht University
P.O. Box 80000, 3508, TA, Utrecht, The Netherlands

N. K. Zawacka, Z. Hens
Physics and Chemistry of Nanostructures Group, Department of Chemistry
Ghent University
Technologiepark 126, 9052 Gent, Belgium

P. Leblans
Agfa NV
Septestraat 27, 2640 Mortsel, Belgium

S. Verkuilen
Heijmans Infra
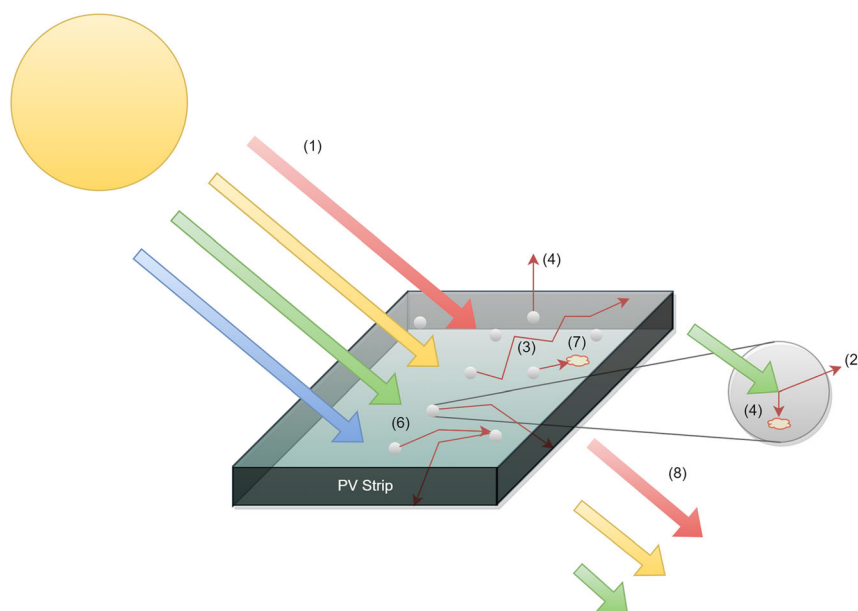Graafsebaan 55, 5248, JS, Rosmalen, The Netherlands

Figure 1. Working principle of a luminescent solar concentrator, irradiance (1) from the sun is incident on the transparent slab and absorbed by the lumino-phores (gray spheres) to be subsequently emitted (2), and part of this will arrive at the sides via total internal reflection (3). Loss mechanisms include escape cone losses (4), quantum yield losses (5), reabsorption by the luminophore (6), and absorption by the waveguide (7). The light which is not absorbed is transmitted (8).

for a few months.[12] Up to date, a long-term outdoor performance analysis of large-area QDLSCs is still lacking.

Despite this research gap, outdoor testing of LSCs started as early as 1985, focusing on daily fluctuations.[13] In the late 1990s, some studies reported similar results[14,15] while also deepening the understanding of photodegradation in an outdoor environment.[15,16] Due to the sharp decrease in price for conventional solar cells, outdoor LSC research stagnated for about 15 years until mid-2010, when LSC research accelerated.

Current outdoor performance research focuses on daily power output fluctuations,[3,12,17–23] long-term fluctuations,[17,20,24] and degradation.[17,19,21,25,26] All of those articles have used organic dyes, predominately Lumogen F Red 305. LSCs based on QDs have not seen as much research in outdoor conditions besides the aforementioned $CuInS_2$ QDLSCs by Makarov et al.[12]

In this work, we compare the daily fluctuations and the 1-year performance of luminescent solar concentrators based on three different quantum dots (CdSe/CdS/ZnS, CuInS2/ZnS, and InP/ZnSe/ZnS core/shell quantum dots) to two reference LSCs (one containing Lumogen F Red 305 as luminophore and a blank without any luminophore). First, the Experimental Section briefly describes the synthesis of the QDs, the construction of LSCs, and the recording and analysis of the data. The results section shows the characterization of the LSCs, their performance on a cloudy day, with primarily diffuse irradiance, and on a sunny day, with mostly direct irradience, and compares the performance of QDLSCs to that of the reference LSCs. Furthermore, the long-term stability of QDLSCs is assessed over an entire year and compared with the trends observed in a photodegradation study of over 400 h. For readability purposes, we refer to the QDs-based LSCs by the composition of their core ("CdSe," "CuInS₂," and "InP") and Lumogen F Red 305 as "Lumogen."

2. Experimental Section

2.1. Fabrication of the LSCs

The Lumogen F Red 305 dye was purchased from BTC Europe GmbH. The QDs were prepared according to the following literature procedures: CdSe/CdS/ZnS[27,28] CuInS₂/ZnS, and InP/ZnSe/ZnS.[29]

Four LSCs were fabricated by dispersing the luminophore of interest in a Kraton-based resin. Then, using a system built in house at Agfa NV with an Elcometer 3530 film applicator, the mixture was doctor bladed on top of a $50 \times 60 \times 0.6\ cm^3$ poly(methyl methacrylate) (PMMA) slab purchased from Arkema (Altuglas). The blade speed was $1.4\ cm\ s^{-1}$. An identical PMMA slab was placed on top of the doctor-bladed film to encapsulate the luminophore-containing Kraton layer. The fifth device, the blank, was prepared following the same procedure but without a luminophore in the Kraton layer. The assembled LSCs were cut to $45 \times 50\ cm^2$ for the outdoor setup. The remaining pieces were used for the optical characterization of the devices and the photodegradation study. Four CIGS photovoltaic (PV) strips (10 cells of $4.5 \times 1\ cm^2$ in series, from Miasole) were coupled to each side of the LSCs with a transparent double-sided acrylic tape, for a total of twenty PV strips (averaged data: $\eta = 13.35\%\ (\sigma_\eta = 0.273)$, FF $= 71.02\%\ (\sigma_{FF} = 1.42)$, see Table S1, Supporting Information). I–V curve fitting using a one-diode model with a diode quality factor of 1 was performed, from which series and shunt resistance values were obtained.[30]

2.2. Characterization of the LSCs

Before outdoor exposure, the power conversion efficiency (PCE) of each large-area LSC was characterized under standard test

conditions (STC) (AM1.5 G (1000 W m^{-2}) at 25 °C) using a vertical Eternal Sun solar simulator, with a black background (following procedures in the study by Yang et al.[31]). PCE data per PV strip (PCE in the LSC STC (%)) are listed in Table S1, Supporting Information.

The light transmission of 2×2 cm^2 fractions of the LSCs was measured on a double-beam PerkinElmer Lambda 950 UV/Vis/NIR spectrometer with no reference sample.[32] The average visual transmittance (AVT) was calculated according to Yang et al.[32] The luminescence spectra were acquired on an Edinburgh Instruments FLS920 spectrofluorometer equipped with double-grating monochromators in the excitation and the emission paths, a 900 W Xe lamp as the excitation source, and an R928 photomultiplier (PMT). The samples were excited at 450 nm, and a 500 nm long-pass filter was placed before the entrance slit of the emission monochromator. The raw data were corrected for the instrumental response.

The photodegradation of 2×2 cm^2 pieces of the LSCs was characterized in a customized setup (Figure S1A, Supporting Information). The pieces were exposed frontally to a cold light source (KL 2500 LED from SCHOTT, 80 W) for up to 420 h, only interrupted to keep track of the degradation. The setup allowed for the illumination of three samples simultaneously. The transmittance and luminescence of the samples were monitored over time, waiting for 5 min in the dark before the measurements. The transmittance was measured as described in the paragraph earlier. The luminescence, instead, was measured in a homemade optical setup (Figure S2A, Supporting Information) using a halogen lamp (DH-2000 from Ocean Optics, 20 W) as the excitation source to prevent further degradation while characterizing the sample. The LSC was illuminated frontally, and the emitted light was collected by a collimating lens coupled to an optical fiber and an HR4000 spectrometer (Ocean optics). The data acquired were corrected for the instrumental response.

2.3. Support Structure and Orientation

The fabricated LSC plates were mounted vertically in an aluminum frame and subsequently placed 5 m above ground on top of a solar noise barrier test setup (**Figure 2**A) in a north–south orientation (Figure 2B). Each PV strip was attached to an EKO Europe IV-tracer via two 12-channel multiplexers using 25 *m*-long cabling. Full *I–V* curves were measured every 2 min, from which short-circuit current (I_{sc} (A)), open-circuit voltage (V_{oc} (V)), maximum power point (P_{mpp} (W)), fill factor (FF), current at *mpp* (I_{mpp} (A)), and voltage at mpp (V_{mpp} (V)) were determined. Due to instrument restrictions, 18 of the 20 cells could be measured: the north and south PV strips of the Blank LSC were not connected. Furthermore, a pyranometer was placed nearby to measure global horizontal irradiance (GHI, in W m^{-2}).

2.4. Efficiency Calculations

The PCE of an LSC is defined according to Equation (1), adapted from ref. [33].

$$\text{PCE} = \frac{P_{\text{out}}}{P_{\text{in}}} = \frac{\sum_i P_{\text{mpp}}(i)}{A_{\text{LSC}} \sum_K E_{s,c}} \tag{1}$$

Here the sum of the maximum power points (MPP) of the PV strips (i) per LSC is taken as the power out. For power in, A_{LSC} is the surface area of the LSC (m^2), and E is the irradiance incident on the LSC (W m^{-2}). The irradiance is the sum of the LSC surface sides s (f: front, b: back) and c the component of incident light (dir: direct, sky-dif: sky-diffuse, ground-dif: ground-diffuse). Summation of K consists of the following set of sets: $K = [$(f, dir), (b, dir), (f, sky-dif), (b, sky-dif), (f, ground-dif), (b, ground-dif)$]$.

After obtaining GHI from the local pyranometer, the Erbs decomposition model[34] was used to obtain the diffuse and direct components. The calculated direct, sky-diffuse, and ground-diffuse components were subsequently transformed to plane-of-array irradiance for both sides of the LSC. These transpositional calculations were based on the Perez model.[35] The ground Albedo was assumed to be constant at 0.2. The calculations were similar to those done for bifacial PV.[36]

3. Results

3.1. Characterization of the LSCs

The absorption and emission spectra of the LSCs are shown in **Figure 3**A. The absorbance was measured using the unhindered light beam as the reference. Hence, the minimum absorption value is 0.04 (92% of transmission) because of reflection losses. Figure 3B shows the sandwich structure of the LSC.

Note that the effective area of the LSC is 43×48 cm^2 for the outdoor measurements since the support frame blocks 1 cm at the edges of the LSC. In the indoor STC measurement setup, this blockage of the support structure was not present. The Kraton layer has a thickness of 50 μm (Figure 3B). The acrylic tape is transparent to the emitted photons by the luminophores (Figure S3A, Supporting Information). Similarly, the CIGS strips have maximum external quantum efficiency in the same range, optimizing the performance of the device (Figure S3B, Supporting Information).

Figure 4 shows the PCE and AVT for the LSCs measured at STC conditions. As expected, the efficiency decreases with increasing AVT. The Lumogen LSC has the highest PCE value with 0.6 % due to its characteristic bright emission and broad absorption across the solar spectrum.[37] The second-best performer is the CdSe LSC, despite having a higher AVT than CuInS$_2$ and InP LSCs. We attribute this to the weak absorption at wavelengths longer than 500 nm and higher luminescence efficiency. The third highest efficiency is 0.4% for the CuInS$_2$ LSC. The QDLSC with the lowest efficiency is the InP LSC with 0.2%. The blank LSC performs worse than any of the other devices, with a PCE of 0.15%.

Comparing the obtained PCE values to similar devices reported in literature is hard. Most research concerns smaller devices or does not report PCE values.[5] However, ref[18] reports on a 50×50 cm^2 LSC based on DTB and DPA dyes with a PCE of 1.03%. Unfortunately, some essential information (AVT, I_{SC}, V_{OC}) is missing to allow for a detailed comparison.

Figure 2. A) Test setup near Rosmalen in The Netherlands, the tinted rectangles at the top of the structure are the LSCs described in this article. The photo was taken on 10 February 2021. B) The orientation of the LSC support structure, the numbers correspond to the following luminophores: 1) InP, 2) CuInS$_2$, 3) CdSe, 4) Lumogen, 5) Blank. The red arrow of the compass at the top left of the picture points toward the geographical North.
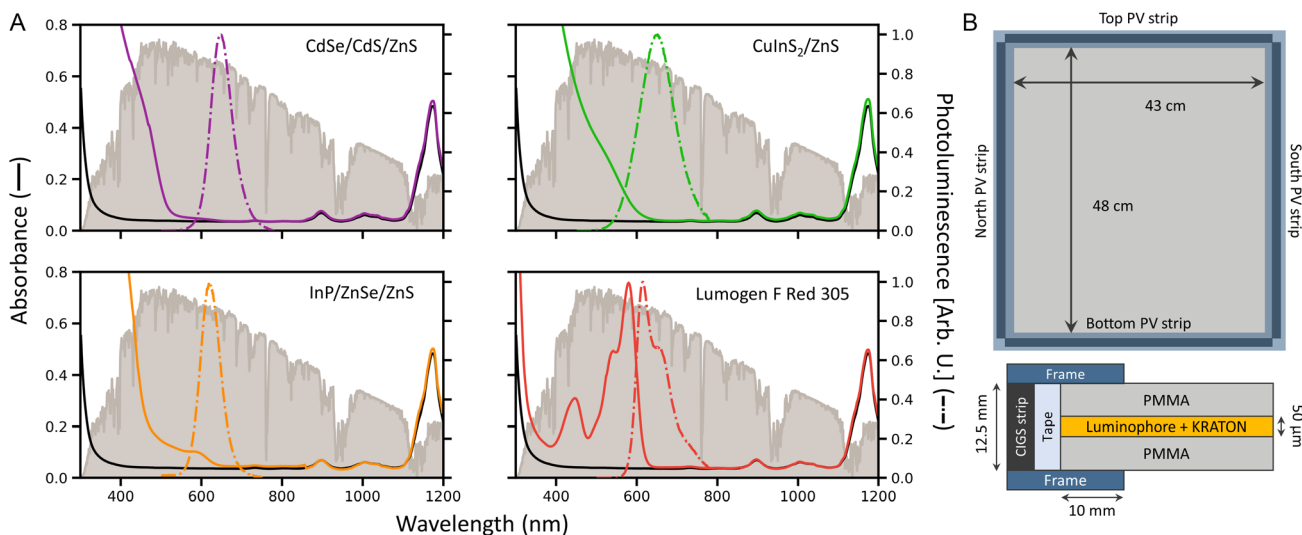

Figure 3. A) Absorption and emission spectra of the luminophore-based LSCs (colored lines). For comparison, the absorption spectrum of the blank LSC is shown in each of the panels (black line). The AM1.5 G spectrum (W m^{-2}) is shown in the background (gray area). B) Frontal view and cross section of the fabricated LSCs with the characteristic dimensions. The blue frame blocking part of the waveguide is present in the outdoor setting and was not present during STC measurements.

A study by UbiQD[12] reported on LSCs with $30 \times 30\,cm^2$, $40 \times 40\,cm^2$, and $50 \times 50\,cm^2$, among other sizes, and showed external quantum efficiencies between 6.4% and 3.1%. A QDLSC ($30 \times 30\,cm^2$) using CuInS$_2$ QDs was constructed by ref. [11] showing an optical power efficiency of 6.4%.

3.2. Efficiencies During a Day

A cloudy day (6 February 2021) and a sunny day (24 February 2021) have been analyzed to assess the daily performance fluctuations of the LSCs. Cloudy days are characterized by
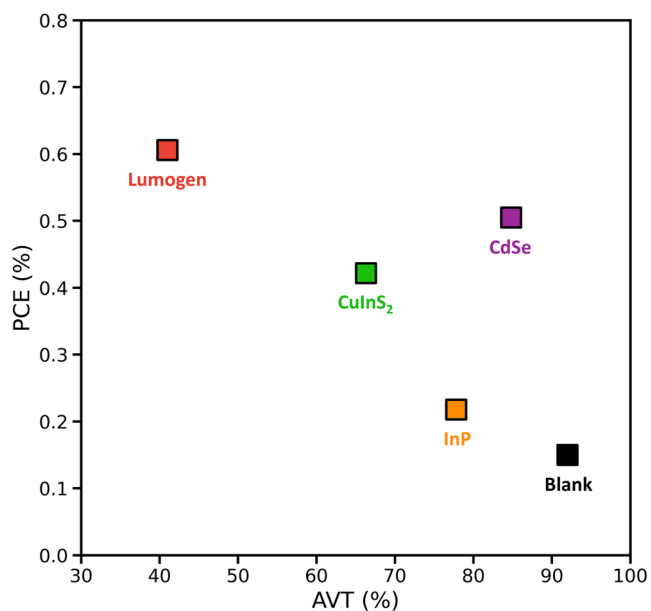
Figure 4. PCE and AVT of the fabricated LSCs; the figures of merit of an LSC. See details for the definition of AVT in ref. [48].

predominantly diffuse irradiance and sunny days by direct irradiance. **Figure 5** shows the efficiency according to Equation (1). For both days, $CuInS_2$ performs the best, followed by Lumogen and CdSe, and the worst efficiencies are obtained for the InP-based QDLSC. The blank LSC shows little-to-no power output. Note that timesteps with $GHI \leq 15\,W\,m^{-2}$ have been removed to avoid outliers.

Figure 5A shows the efficiency on a cloudy day. Since the irradiance is incident as from an isotropically emitting half-sphere, the irradiance, while fluctuating, stays mostly constant over the day. The support structure seems to have little influence on the efficiency of the LSCs during the cloudy day.

In contrast, for the sunny day, Figure 5B, the support structure has a clear effect. At noon, the support structure blocks the direct irradiance on the LSC since it is oriented along the North–South line. **Figure 6** shows this concept in detail. The highest efficiencies are obtained in the morning and afternoon when irradiance directly impinges on the LSC. Notable is the similarity between the average efficiencies of the cloudy and sunny day: the average efficiencies for the luminophores for the cloudy and sunny day are, respectively, $CuInS_2$: 0.118% and 0.184% ($\sigma_\eta = 0.024$ and 0.17), Lumogen: 0.07% and 0.09% ($\sigma_\eta = 0.019$ and 0.10), CdSe: 0.072% and 0.062% ($\sigma_\eta = 0.018$ and 0.067), and InP: 0.027% and 0.038% ($\sigma_\eta = 0.0084$ and 0.031). The similarity of LSC efficiencies for cloudy and sunny days is unlike conventional PV, which sees a drop in performance under diffuse irradiance. The individual power outputs for the PV strips are further analyzed to investigate the effect of irradiance.

3.3. Power Outputs per PV Strip for Cloudy and Sunny Day

Figure 7 and **8** show the power output per PV strip for the cloudy and sunny day, respectively. Figure 7 shows higher power outputs for the bottom and north PV strips on the cloudy day. This can be understood because the diffuse irradiance can be modeled by an isotropically emitting half sphere. As a result, the bottom PV strip will perform better than the other PV strips, as visible from the blank bottom and blank top PV strip. The
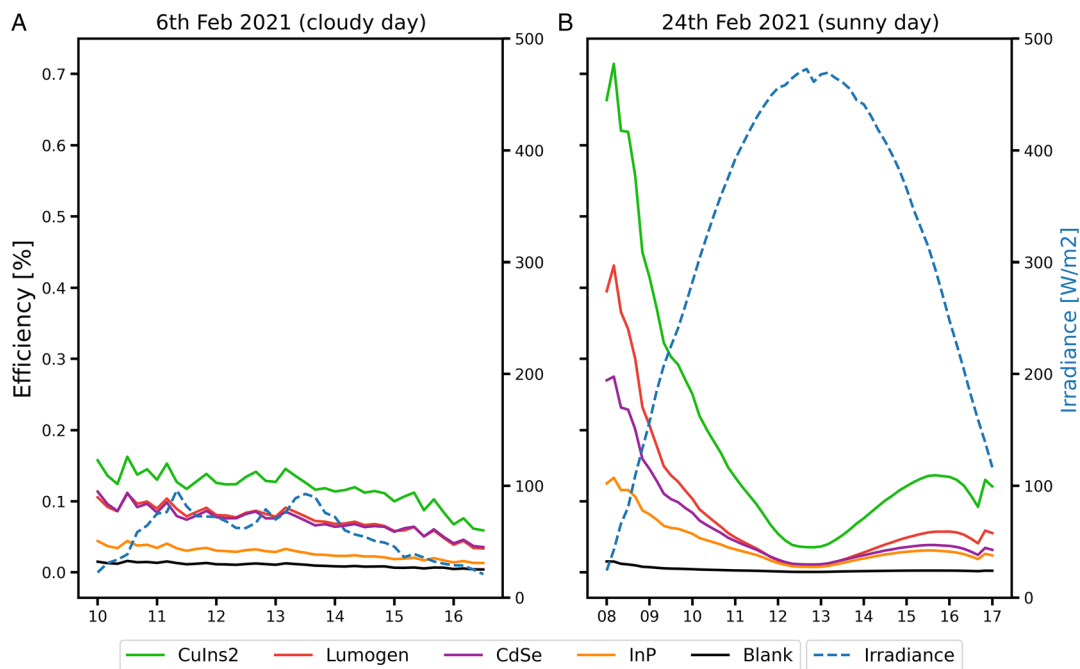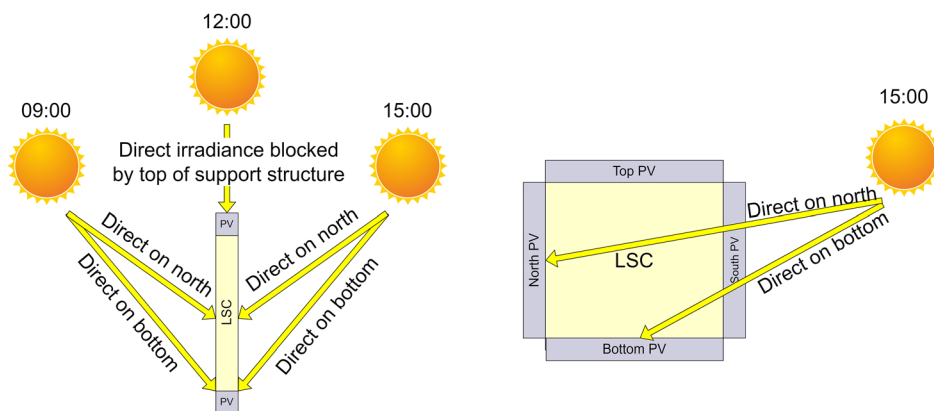

Figure 5. Efficiency of the LSCs during a A) cloudy day (6 February 2021) and B) a sunny day (24 February 2021). The blank LSC without a luminophore is indicated by the black line. The blue dashed line indicates GHI on both days.

ADVANCED
SCIENCE NEWS
www.advancedsciencenews.com

Solar
RRL
www.solar-rrl.com

Figure 6. Influence of direct irradiance on the power output on the North and bottom strips. Direct irradiance on the North and bottom strips will increase the power output in the morning and the afternoon.
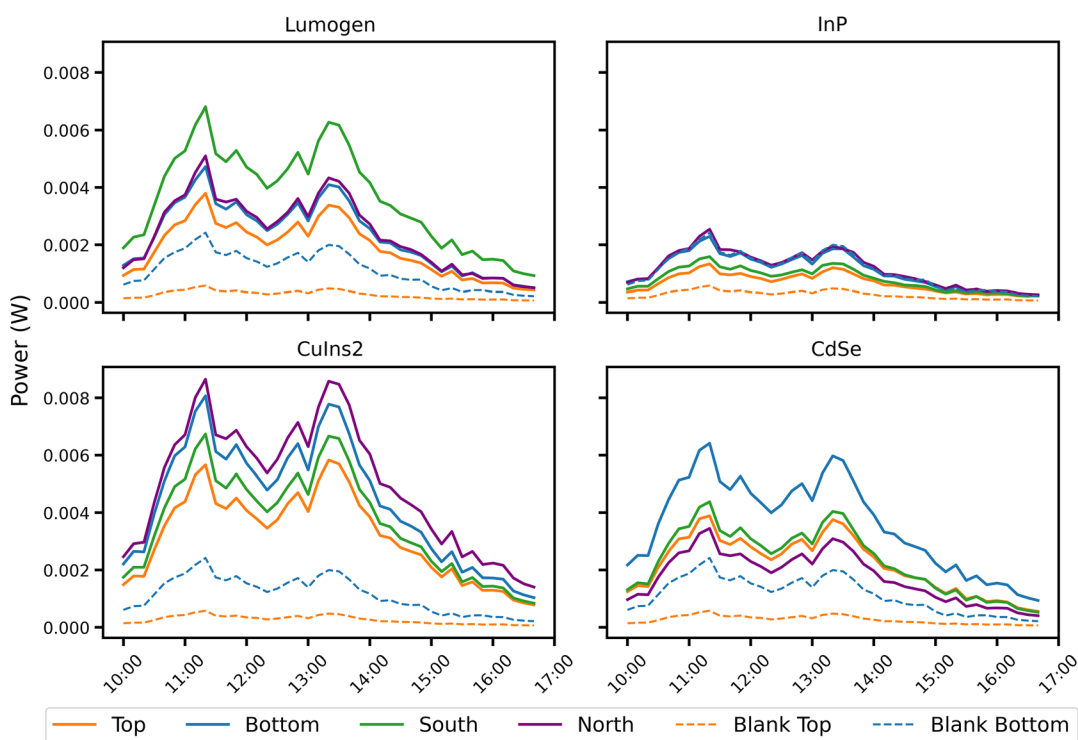

Figure 7. Power output per PV strip on a cloudy day (6 February 2021). For details on the orientation of the PV strips, see Figure 3.

increased power output of the north strips is probably due to some direct irradiance, despite the clouds.

The PV strip characteristics explain differences in the power output between solar strips not explained by direct irradiance or LSC characteristics. The irradiance falling on the PV strips attached to an LSC is low compared to direct irradiance under STC. Table S1, Supporting Information, shows the characteristics of the used PV strips (PV strip STC efficiency (%), FF, PCE in the LSC STC (%), and shunt resistance (Ohm)). Following ref. [38], a low shunt resistance is associated with decreased performance at low irradiance values. This effect is visible for the south-facing strip of the Lumogen LSC that outperforms the other PV strips attached to the Lumogen LSC; it has a relatively high shunt resistance of

917.5 Ohm. Furthermore, the bottom strip of the CdSe LSC outperforms the other PV strips with a shunt resistance of 948.6 Ohm.

The power output differences per PV strip for a sunny day, see Figure 8, show a strong influence of direct irradiance on the power output of the north strips. Especially CuInS$_2$ and InP show a high relative power output increase for the north strip. For Lumogen and CdSe, the north strips do not have a substantial power output increase since the PV strips have a lower shunt resistance than the other PV strips; see Table S1, Supporting Information. This effect was also visible on a cloudy day in Figure 7. Additionally, because of the North–South orientation, two peaks can be seen.
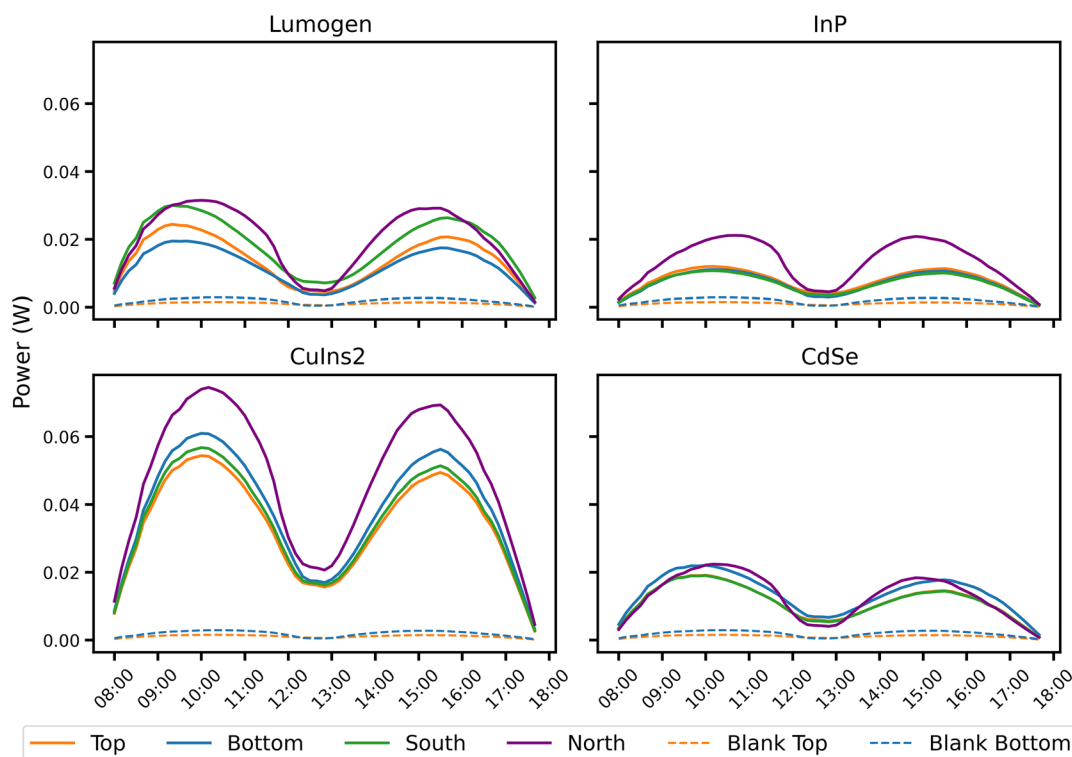
Figure 8. Power output per PV strip on a sunny day (24 February 2021). For details on the orientation of the PV strips, see Figure 3.
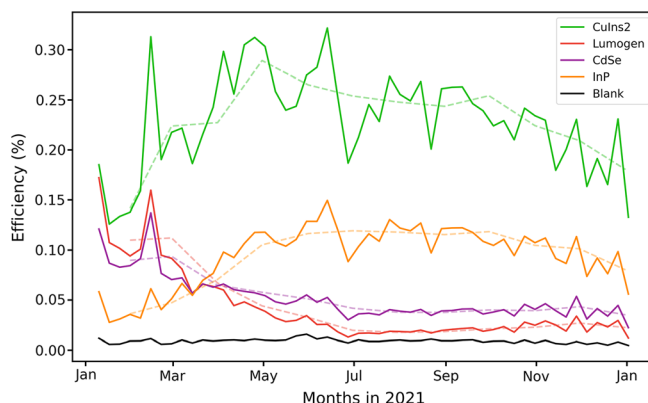

Figure 9. Monthly (dashed line) and weekly (solid line) average efficiency over a year for all the luminophores and the blank LSC.

3.4. Efficiency Over a Year

The selected date of the cloudy and sunny day was purposely early in the experiment to avoid the effect of degradation of the luminophores. Studying this effect is the second goal of the article. **Figure 9** shows the weekly and monthly average efficiency of the luminophores over a year. It is clear that the change in efficiency is highly dependent on the luminophore.

The efficiencies for $CuInS_2$ and InP LSCs both increase in the summer, while the efficiency of the Lumogen and CdSe LSCs decreases quickly after their inception in February. Outdoors, the LSCs are exposed to UV light, temperature changes, and

moisture that can cause degradation of the luminophores and the waveguides. Environmental factors could explain the decrease in performance but cannot account for the improvements observed.

The increase in efficiency for $CuInS_2$ and InP potentially results from higher irradiance during summer. Low irradiance values are associated with low efficiencies for conventional PV cells,[38] especially since shunt resistances are not very high. However, the temperature increase during summer will have an inverse effect on the efficiency of the PV strips.

A third possibility is the photobrightening of the QDs as a result of filling the thermodynamic unfavorable defect states. Figure S4, Supporting Information, shows the normalized efficiency, relative

to that of 17 January 2021 (the start of the experiments), and shows a significant increase in efficiency of ≈ 180% and ≈ 300% for CuInS$_2$ and InP, respectively. To investigate this effect, a laboratory study on photodegradation is conducted.

3.5. Photodegradation Study

To test the hypothesis of degradation and photobrightening of the luminophores, small leftover pieces kept in the dark for two years were exposed to white LEDs, and their optical properties were measured over time. The setup allows for the illumination of three samples simultaneously, although at unequal intensities. Hence, the degradation rates observed are not trivial to compare (Figure S1B, Supporting Information). The luminescence measured for the InP and CuInS$_2$ LSCs changed before the white light illumination. For that reason, the earliest measurement under illumination (1.5 h) was taken as the reference value. This surprising observation is discussed below.

Within the first 24 h, the luminescence of all three QDLSCs increased with respect to their intensity after 1.5 h of illumination (**Figure 10**A). For the Lumogen LSC, there is 11 % reduction in luminescence. At longer times, the luminescence of CuInS$_2$ and InP kept increasing up to 1.7 and 4.0 times, respectively (Figure 10B). The initial enhancement observed for the CdSe LSC reversed after one day of illumination, decreasing to 70% of the initial value after 420 h. The performance of the Lumogen LSC consistently decreased during the experiment. The luminescence is the driving force of an LSC and is directly related to the efficiency of the device. The trends observed in the photodegradation experiment qualitatively match the outdoor performance evolution (Figure S5, Supporting Information).

We look at the evolution of the absorption and emission spectra to understand the changes observed in the photodegradation experiment. The full spectra can be found in Figure 6–9. During illumination, the characteristic absorption band of PMMA at 1174 nm remains unchanged in all the LSCs, proving that PMMA has not degraded. Lumogen is the only luminophore whose characteristic absorption band decreased over time, a signature of photodegradation (Figure S6A, Supporting Information). Interestingly, the absorption and emission reductions have a decay rate of 2010 ± 328 and 445 ± 165 h, respectively (insets Figure S6, Supporting Information). The dye degradation occurs slower than

the luminescence quenching. Minor photon-induced chemical modifications of Lumogen with the embedding matrix could explain the preservation of the optical transition's intensity while increasing the nonradiative decay rate. Despite having a slower photodegradation rate than similar organic dyes,[39] it is evident that Lumogen can photodegrade when embedded in a polymeric matrix.[21,40–42] It is noteworthy that Lumogen can degrade even in the absence of UV light[21,40,41] or laser pulses.[42]

All QDLSCs show no decrease in absorbance after 420 h of illumination, indicating that the QDs have not degraded. It is known that the luminescence of QDs can be enhanced or quenched upon illumination, respectively, known as photobrightening and photodarkening.[43] In the case of CdSe, the initial luminescence increase and subsequent decrease occur at a constant spectral shape (Figure S7B, Supporting Information). The absence of a blueshift when quenched excludes photo-oxidation of the QDs as the cause.[44] Instead, the luminescence quenching can be explained by the increasing fraction of QDs in a dark state.[43]

Regarding the InP and CuInS$_2$ QDs, their response to prolonged light exposure is considerably less studied than for CdSe. The InP and CuInS$_2$ LSCs experienced a drop in luminescence after 1.5 h of white light illumination. To ensure the luminescence measurements had a small impact on the photodegradation process, a halogen lamp with a weak blue light component was used as the excitation source (Figure S2B, Supporting Information). This approach resulted in stable luminescence spectra for all the samples, including time zero measurements. The luminescence intensity of the InP QDLSC initially dropped by 10 % and rapidly recovered and increased above the initial value, with constant peak position (Figure S8B, Supporting Information). The emission spectra show a weak and broad band above 700 nm that is attributed to emission from a trap state.[45] Interestingly, the intensity of this feature decreases during illumination, suggesting that charge carrier traps are being filled or removed. At the ensemble level, Dussert et al.[46] also reported photobrightening of InP/ZnSe/ZnS QDs during accelerated aging in aqueous solution, although for only 15 min before quenching and blueshifting start. The constant peak position observed here suggests that the QDs are not degrading. At the single-particle level, it has been found that under continuous illumination, the fraction of InP/ZnS QDs
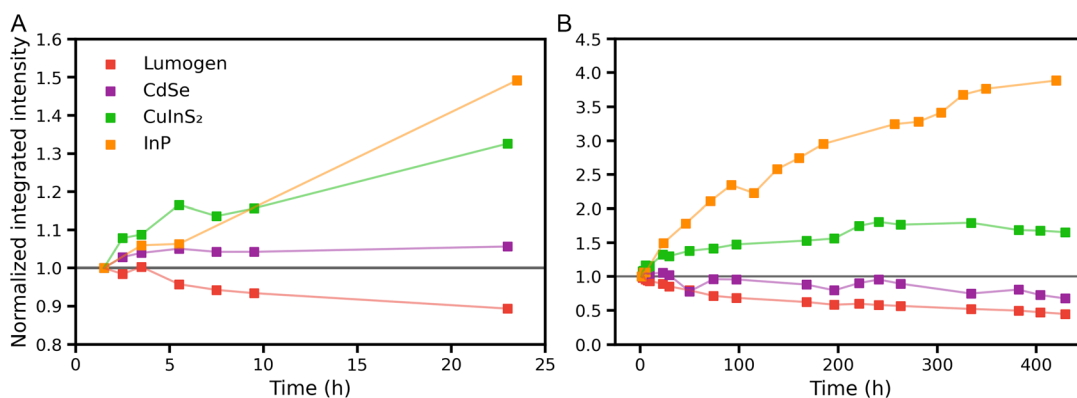

Figure 10. Integrated luminescence intensity normalized by the measured intensity after 1.5 h of illumination. A) First 24 h of illumination. B) Full extension (420 h) of the experiment.

in the bright state increases over time, providing evidence of photobrightening in this material.[47]

In contrast to the InP QDLSC, the initial luminescence drop of 50% observed for the $CuInS_2$ QDLSC is not fully recovered in the photobrightening phase (Figure S9B, Supporting Information). The initial drop in intensity is accompanied by a peak blueshift of 5.5 nm (17 meV). At constant illumination, the luminescence increases, and its maximum is redshifted by 9 nm (27 meV). The QDs' ensemble inhomogeneities can explain this result. Since their optoelectronic properties strongly depend on the size, any size-sensitive transformation will affect smaller and larger QDs within the ensemble differently. Nevertheless, the origin of the photodarkening and photobrightening observed in the QDLSCs is not yet fully understood and will be the subject of follow-up studies.

4. Conclusion

This study analyzed the outdoor performance of three quantum dot-based luminescent solar concentrators and compared them to two reference LSCs: a Lumogen LSC and a blank LSC without a luminophore. The highest PCE of the QDLSCs under STC was obtained for the CdSe LSC with a value of 0.5%, followed by $CuInS_2$ and InP LSCs with 0.4% and 0.2%, respectively. The Lumogen had the highest efficiency of 0.6%, and the Blank LSC had the lowest with 0.15%.

The daily power output results showed a stable efficiency under diffuse irradiance, in line with LSC research.[3] For a sunny day, the orientation of the support structure along the North–South line resulted in a blockade of the sun around noon and, consequently, a drop in efficiency. Another result of the orientation is the increase in power output for the North and Bottom PV strip due to direct irradiance. Differences between solar strips not explained by direct irradiance are related to differences in shunt resistance per PV strip, based on ref. [38] High shunt resistances are thus an essential property of PV strips/cells attached to LSCs.

Interestingly, the PCE of the LSCs evolved during the 1 year outdoor exposure. For the $CuInS_2$- and InP-based QDLSCs, the efficiency improved by 80% and 200% since January 17th, 2021. On the contrary, the CdSe QDLSC experienced a 40% drop in efficiency, while the Lumogen LSC lost 60% of its initial performance. These trends are reproduced by the photodegradation study, providing evidence of photobrightening, luminescence quenching, and the absence of degradation in the QDLSCs. Future studies should look into a postmortem analysis for details on the degradation of the LSCs.

Supporting Information

Supporting Information is available from the Wiley Online Library or from the author.

Acknowledgements

Conflict of Interest

The authors declare no conflict of interest.

Author Contributions

T.A.B. took care of writing the manuscript, data analysis, daily and long-term performance, and conceptualization. R.T.-P. took care of writing the manuscript, characterization of the LSC plates, photodegradation experiment, and data analysis. A.K. took care of writing the manuscript, data analysis, daily and long-term performance, and conceptualization. N.K.Z. took care of synthesis of the QDs and fabrication of the LSC plates. P.T.P. took care of characterization of the LSC plates. T.F.J.G. took care of data analysis daily and long-term performance and conceptualization. A.C.W. took care of attaching solar cell strips to LSC plates and data acquisition. D.K.G.B. took care of reviewing of the manuscript and experimental advice. D.A.M.V. took care of reviewing of the manuscript and supervision. P.L. took care of fabrication of LSC plates. S.V. took care of realization of the outdoor test setup. Z.H. took care of design of the experiments, supervision of the synthesis of the QDs, and fabrication of the LSC plates. C.M.D. took care of design of the experiments, supervision of the characterization of the LSC plates and photodegradation experiment, and writing of the manuscript. W.G.J.H.M.S. took care of design of the experiments, attaching solar cell strips to LSC plates, mounting of the LSC plates in the outdoor framework, data acquisition, data analysis, writing of the manuscript, conceptualization, and overall coordination.

Data Availability Statement

The data that support the findings of this study are available from the corresponding author upon reasonable request.

Keywords

[1] W. G. v. Sark, K. W. Barnham, L. H. Slooff, A. J. Chatten, A. Büchtemann, A. Meyer, S. J. McCormack, R. Koole, D. J. Farrell, R. Bose, E. E. Bende, A. R. Burgers, T. Budel, J. Quilitz, M. Kennedy, T. Meyer, C. D. M. Donegá, A. Meijerink, D. Vanmaekelbergh, *Opt. Express* **2008**, *26*, 21773.

[2] M. G. Debije, P. P. C. Verbunt, *Adv. Energy Mater.* **2012**, *2*, 12.

[3] M. G. Debije, V. A. Rajkumar, *Sol. Energy* **2015**, *122*, 334.

[4] C. Yang, M. C. Barr, R. R. Lunt, *Phys. Rev. Appl.* **2022**, *17*, 034054.

[5] J. Roncali, *Adv. Energy Mater.* **2020**, *10*, 2001907.

[6] P. Moraitis, R. Schropp, W. van Sark, *Opt. Mater.* **2018**, *84*, 636.

[7] P. Reiss, M. Protiere, L. Li, *Small* **2009**, *5*, 154.

[8] A. Kim, A. Hosseinmardi, P. K. Annamalai, P. Kumar, R. Patel, *Chem. Select* **2021**, *6*, 4948.

[9] J. Bomm, A. Büchtemann, A. J. Chatten, R. Bose, D. J. Farrell, N. L. Chan, Y. Xiao, L. H. Slooff, T. Meyer, A. Meyer, W. G. J. H. M. van Sark, R. Koole, *Sol. Energy Mater. Sol. Cells* **2011**, *95*, 2087.

[10] B. Liu, S. Ren, G. Han, H. Zhao, X. Huang, B. Sun, Y. Zhang, *J. Mater. Chem. C* **2021**, *9*, 5723.

[11] A. Anand, M. L. Zaffalon, G. Gariano, A. Camellini, M. Gandini, R. Brescia, C. Capitani, F. Bruni, V. Pinchetti, M. Zavelani-Rossi, F. Meinardi, S. A. Crooker, S. Brovelli, *Adv. Funct. Mater.* **2020**, *30*, 1906629.

[12] N. S. Makarov, D. Korus, D. Freppon, K. Ramasamy, D. W. Houck, A. Velarde, A. Parameswar, M. R. Bergren, H. McDaniel, *ACS Appl. Mater. Interfaces* **2022**, *14*, 29679.

[13] M. S. de Cardona, M. Carrascosa, F. Meseguer, F. Cusso, F. Jaque, *Appl. Opt.* **1985**, *24*, 2028.

[14] A. F. Mansour, *Polym. Test.* **1998**, *17*, 153.

[15] A. F. Mansour, A. L. Salem, N. M. El-Sayed, A. H. Bassyouni, *Proc. Indian Acad. Sci. Chem. Sci.* **1998**, *110*, 351.

[16] M. A. El-Shahawy, A. F. Mansour, *J. Mater. Sci. Mater. Electron.* **1996**, *7*, 171.

[17] S. M. El-Bashir, O. A. AlHarbi, M. S. AlSalhi, *Int. J. Photoenergy* **2013**, *2013*, 1.

[18] N. Aste, L. C. Tagliabue, C. Del Pero, D. Testa, R. Fusco, *Renew. Energy* **2015**, *76*, 330.

[19] C. Corrado, S. W. Leow, M. Osborn, I. Carbone, K. Hellier, M. Short, G. Alers, S. A. Carter, *J. Renew. Sustain. Energy* **2016**, *8*, 043502.

[20] M. Kanellis, M. M. de Jong, L. Slooff, M. G. Debije, *Renew. Energy* **2017**, *103*, 647.

[21] J.-M. Delgado-Sanchez, *Sol. Energy Mater. Sol. Cells* **2019**, *202*, 110134.

[22] A. Sethi, S. Chandra, A. Ortega, S. McCormack, *Plasmonics* **2022**, *17*, 725.

[23] Y. Nie, W. He, X. Liu, Z. Hu, H. Yu, H. Liu, *Build. Simul.* **2022**, *15*, 1789.

[24] M. G. Debije, C. Tzikas, M. M. de Jong, M. Kanellis, L. H. Slooff, *Renew. Energy* **2018**, *116*, 335.

[25] L. H. Slooff, N. J. Bakker, P. M. Sommeling, A. Büchtemann, A. Wedel, W. G. J. H. M. van Sark, *Phys. Status Solidi A* **2014**, *211*, 1150.

[26] S. M. El-Bashir, I. Yahia, F. Al-Harbi, H. Elburaih, F. Al-Faifi, N. A. Aldosari, *Int. J. Green Energy* **2017**, *14*, 270.

[27] D. V. Talapin, I. Mekis, S. Götzinger, A. Kornowski, O. Benson, H. Weller, *J. Phys. Chem. B* **2004**, *108*, 18826.

[28] L. Li, A. Pandey, D. J. Werder, B. P. Khanal, J. M. Pietryga, V. I. Klimov, *J. Am. Chem. Soc.* **2011**, *133*, 1176.

[29] Y. Li, X. Hou, X. Dai, Z. Yao, L. Lv, Y. Jin, X. Peng, *J. Am. Chem. Soc.* **2019**, *141*, 6448.

[30] A. Polman, W. G. J. H. M. van Sark, W. C. Sinke, F. W. Saris, *Sol. Cells* **1986**, *17* 241.

[31] C. Yang, H. A. Atwater, M. A. Baldo, D. Baran, C. J. Barile, M. C. Barr, M. Bates, M. G. Bawendi, M. R. Bergren, B. Borhan, C. J. Brabec, S. Brovelli, V. Bulović, P. Ceroni, M. G. Debije, J.-M. Delgado-Sanchez, W.-J. Dong, P. M. Duxbury, R. C. Evans, S. R. Forrest, D. R. Gamelin, N. C. Giebink, X. Gong, G. Griffini, F. Guo, C. K. Herrera, A. W. Ho-Baillie, R. J. Holmes, S.-K. Hong, T. Kirchartz, et al., *Joule* **2022**, *6*, 8.

[32] C. Yang, D. Liu, M. Bates, M. C. Barr, R. R. Lunt, *Joule* **2019**, *3*, 1803.

[33] Á. Bognár, S. Kusnadi, L. H. Slooff, C. Tzikas, R. C. Loonen, M. M. de Jong, J. L. Hensen, M. G. Debije, *Renew. Energy* **2020**, *151*, 1141.

[34] D. Erbs, S. Klein, J. Duffie, *Sol. Energy* **1982**, *28*, 293.

[35] R. Perez, P. Ineichen, R. Seals, J. Michalsky, R. Stewart, *Sol. Energy* **1990**, *44*, 271.

[36] R. O. Yakubu, M. T. Ankoh, L. D. Mensah, D. A. Quansah, M. S. Adaramola, *Energies* **2022**, *15*, 22.

[37] G. Seybold, G. Wagenblast, *Dyes Pigm.* **1989**, *11*, 303.

[38] N. H. Reich, W. G. J. H. M. van Sark, E. A. Alsema, R. W. Lof, R. E. I. Schropp, W. C. Sinke, W. C. Turkenburg, *Sol. Energy Mater. Sol. Cells* **2009**, *93*, 1471.

[39] L. R. Wilson, B. S. Richards, *Proc. of the 23rd European Photovoltaic Solar Energy Conf. and Exhibition* **2008**, 510.

[40] M. G. Hyldahl, S. T. Bailey, B. P. Wittmershaus, *Sol. Energy* **2009**, *83*, 566.

[41] G. Griffini, L. Brambilla, M. Levi, M. Del Zoppo, S. Turri, *Sol. Energy Mater. Sol. Cells* **2013**, *111*, 41.

[42] N. Tanaka, N. Barashkov, J. Heath, W. N. Sisk, *Appl. Opt.* **2006**, *45*, 3846.

[43] M. A. Osborne, S. F. Lee, *ACS Nano* **2011**, *5*, 8295.

[44] W. G. Van Sark, P. L. Frederix, D. J. Van den Heuvel, H. C. Gerritsen, A. A. Bol, J. N. Van Lingen, C. de Mello Donega, A. Meijerink, *J. Phys. Chem. B* **2001**, *105*, 8281.

[45] A. Guzelian, J. B. Katari, A. V. Kadavanich, U. Banin, K. Hamad, E. Juban, A. Alivisatos, R. Wolters, C. Arnold, J. Heath, *J. Phys. Chem.* **1996**, *100*, 7212.

[46] F. Dussert, G. Sarret, K. D. Wegner, O. Proux, G. Landrot, P.-H. Jouneau, P. Reiss, M. Carrière, *Nanomaterials* **2022**, *12*, 3703.

[47] V. Chandrasekaran, M. D. Tessier, D. Dupont, P. Geiregat, Z. Hens, E. Brainis, *Nano Lett.* **2017**, *17*, 6104.

[48] C. J. Traverse, R. Pandey, M. C. Barr, R. R. Lunt, *Nat. Energy* **2017**, *2*, 849.